Macromolecules

Article

pubs.acs.org/Macromolecules

Ionic Conductivity and Self-Assembly in Poly(isoprene-*b*-ethylene oxide) Electrolytes Doped with LiTf and EMITf

G. Zardalidis,[†] E. F. Ioannou,[∥] K. D. Gatsouli,[∥] S. Pispas,[∥] E. I. Kamitsos,*[,∥] and G. Floudas*[,†,‡]

[†]Department of Physics, University of Ioannina, P.O. Box 1186, 451 10 Ioannina, Greece

[‡]Max Planck Institute for Polymer Research, 55128 Mainz, Germany

[∥]Theoretical and Physical Chemistry Institute, National Hellenic Research Foundation, 116 35 Athens, Greece

Supporting Information

ABSTRACT: Diblock copolymers of poly(isoprene-*b*-ethylene oxide), PI-*b*-PEO (IEO), are employed as templates for the development of nanostructured polymer electrolytes by salt-doping. For this purpose, lithium triflate (CF_3SO_3Li, LiTf) and 1-ethyl-3-methylimidazolium trifluoromethanesulfonate ($CF_3SO_3-C_6H_{11}N_2$, EMITf) salts were separately introduced at various [EO]:[salt] ratios. The local structure, nanodomain morphology and ion dynamics of the resulted block copolymer electrolytes were investigated by infrared spectroscopy, X-ray scattering, differential scanning calorimetry and dielectric spectroscopy. The structural investigation revealed strong effects of both LiTf and EMITf salt addition to the copolymer nanodomain morphology. These include transitions between different ordered nanophases and an increased domain spacing. The latter was independent of the kind of salt providing the possibility of studying ion transport under identical nanodomain sizes but in the presence of different interactions. Ionic conductivity in the two systems was fundamentally different. In IEO/EMITf ionic conductivity was much higher and comparable to the PEO/EMITf case. However, in IEO/LiTf, ion conductivity was reduced by a factor of a 100 relative to the PEO/LiTf case. This reflects combined effects of increased interaction parameter and of preferential wetting of electrodes. These results suggest ways for manipulating ion transport in polymer electrolytes.

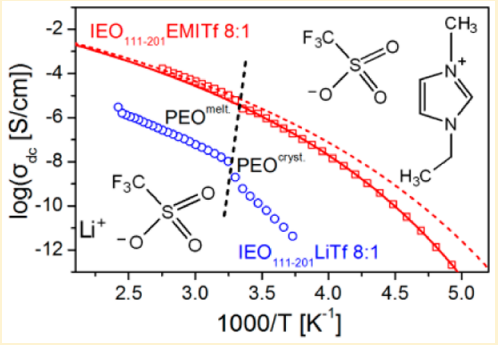

1. INTRODUCTION

Replacing the currently used liquid electrolytes by solid ones recently received considerable attention due to improved safety, wider potential of electrochemical stability and ability for thin film processing. Hence, solid polymer electrolytes (SPE) emerged as promising materials for technological applications including batteries, fuel cells, super capacitors as well as electrochemical devices.[1−4] In particular, the design of SPE from block copolymers with appropriate compositions offers opportunities for such purposes. Such advantages rely on the mechanical strength and propensity for phase separation at the nanoscale.[5] In this respect, the soft nanophase can be employed as an ion conductor, whereas the hard nanophase offers the required mechanical strength.

Poly(ethylene oxide) (PEO) has been employed as one of the blocks because of its flexible backbone and a great ability for solvating salts. Early reports[6,7] on the phase diagram and conductivity[8] behavior of the archetypal PEO-LiX electrolytes (X = $CF_3SO_3^-$, ClO_4^-, AsF_6^-) revealed that below 313 K (the melting point of PEO) these systems are mixtures of different phases. They include a crystalline phase of PEO and a crystalline stoichiometric compound of PEO with the salt (called "complex"), both embedded in amorphous PEO regions. Recently, it was shown[8] that ionic conduction in PEO/LiTf electrolytes takes place both within the stoichiometric complex and in the amorphous phase that is continuously enriched with LiTf ions, with the latter having the major contribution. In addition, ion transport was found to be coupled to local segmental motion of the polymer chains. Extensive research attention was directed on salt doping of PEO-containing block copolymers.[9−19] PEO-based SPEs present a diversity of phases depending on temperature, salt species and salt concentration. Among the different SPEs, the phase behavior of lithium salt-doped poly(styrene-*b*-ethylene oxide) (PS-*b*-PEO) copolymers was extensively investigated as a function of salt LiX concentration and for different counterions (X=ClO_4^-, $CF_3SO_3^-$, AsF_6^-). It was shown that the formation of PEO-salt complexes can lead to changes in nanostructure and domain spacing. More recent studies on PS-*b*-PEO electrolytes as a function of molecular weight revealed that ion conductivity is governed by two competing factors, the glass temperature of the PS phase and the channel width of the conducting PEO phase.[17−19] The presence of two glass temperatures (T_g's) in block copolymers is not a surprise given the level of nanophase separation. Subsequently, self-consistent field theory[20−22] addressed the inhomogeneous

Received: January 15, 2015
Revised: February 17, 2015
Published: February 20, 2015

DOI: 10.1021/acs.macromol.5b00089
Macromolecules 2015, 48, 1473−1482

distribution of Li^+ ions within the conducting phase, the preferential solvation energy of anions, the translational entropy of anions, the ion-pair equilibrium between polymer-bound Li^+ and anion, and the changes in the interaction parameter, χ, due to the bound ions. It was also suggested that long-range order impedes ion transport[17] and that there is a discontinuous increase in conductivity at the order-to-disorder transition temperature reflecting changes in the form factor.[19]

Despite these efforts, ion conductivity of PEO/LiX electrolytes in the neat state as in PEO-based diblock copolymers is still relatively small, with an upper limit of about 10^{-4} S/cm. In this respect, special attention has been drawn to ionic liquids (ILs), i.e., room temperature molten salts composed solely by ions.[23,24] These salts have weak interactions due to the combination of a bulky-asymmetric cation and a "plasticizing anion", that is, an anion having a delocalized charge and multiple conformations differing only slightly in energy. They possess many attractive properties such as low vapor pressure, nonvolatility, nonflammability, high thermal stability, high ionic conductivity, and wide electrochemical stability.[25−28] Furthermore, they are considered as "green solvents", which makes them key materials for the development of a range of emerging technologies.[23] In an effort to combine the excellent properties of ILs with the rubbery compliance of polymers, different types of ILs, such as those with cations based on imidazolium,[26−28] have been used in doping polymers for battery/capacitor applications. The incorporation of ionic liquids in block copolymer electrolytes can influence the segregating behavior of the block copolymers and may lead to enhanced ion transport.[29−33]

In the present study, we explore the effect of salt-doping on the diblock copolymer poly(isoprene-*b*-ethylene oxide) (PI-*b*-PEO) (IEO) system. Lithium trifluoromethanesulfonate salt (CF_3SO_3Li, or lithium triflate-LiTf) and the ionic liquid 1-ethyl-3-methylimidazolium trifluoromethanesulfonate ($CF_3SO_3-C_6H_{11}N_2$, abbreviated as EMITf) were introduced in the PEO phase with varying [EO]:[salt] ratios. We employ this diblock copolymer system for two reasons: (i) the strong segment−segment interaction parameter that describes the free energy cost per monomer of contacts between unlike monomers gives rise to ordered nanodomains even at low molecular weights and (ii) a good knowledge of the bulk phase diagram.[34,35] In their homopolymer state, both polyisoprene and poly(ethylene oxide) have a low glass transition temperature and hence behave as viscous liquids not suitable for solid polymer electrolytes. However, when they combine to form a diblock copolymer, the high interaction parameter leads to an elastic "solid-like" behavior at room temperature.[35] For example, within the crystalline lamellar nanophase the modulus exceeds 10^6 Pa, whereas within the other ordered nanophases shear moduli in the range of 10^5 Pa have been reported.[35] Hence, in doped IEO, an SPE is formed in the presence of two "fluid" nanophases.

The aim of this work is to compare the effect of ionic liquid EMITf versus LiTf salt doping on the self-assembly and ion transport of the same IEO scaffold. By incorporating different salts—bearing the same anion but very different cation sizes—in the same diblock copolymer, we modify the coordination environment of PEO segments, thus, inducing changes in the phase state and domain spacing. We are investigating the effect of these changes on ionic conductivity. The thermodynamics are investigated by differential scanning calorimetry (DSC) and the molecular and supramolecular self-assembly by wide-angle and small-angle X-ray scattering (WAXS/SAXS), respectively. Structural aspects at the atomic/molecular level are explored by infrared spectroscopy (IR), while polymer and ion dynamics are studied by dielectric spectroscopy (DS). We find that the degree of ion association to the PEO backbone dictates the structure and effectively controls ionic conductivity.

2. EXPERIMENTAL SECTION

2.1. Materials. *Block Copolymer Synthesis.* Two poly(isoprene-*b*-ethylene oxide) (PI-*b*-PEO) block copolymers with different compositions and overall molecular weights were synthesized by high-vacuum anionic polymerization techniques.[36] Purification of all reagents (solvents, monomers, etc.) was made according to well-established procedures. The block copolymers were prepared by polymerizing first the isoprene, using s-butyllithium as initiator in benzene, at 298 K, followed by the addition of ethylene oxide to the living polyisoprenyl lithium to give the second block. Ethylene oxide polymerization was conducted at 313 K for 48 h, in the presence of phosphazine base (*t*-BuP_4).[37] The polymerization reaction was then terminated by the addition of degassed methanol to give a symmetric low molecular weight $IEO_{111-201}$ (111 repeats of isoprene and 201 repeats of ethylene oxide) and an asymmetric high molecular weight $IEO_{307-204}$. The desired block copolymers were subsequently isolated by precipitation in methanol/water mixture and dried under vacuum before further use.

The molecular weight and molecular weight distribution for the block copolymers were obtained by size exclusion chromatography, using a Waters system composed of a Waters 1515 isocratic pump, a set of three μ-Styragel mixed bed columns, with a porosity range of 10^2 to 10^6 Å, and a Waters 2414 refractive index detector. The entire system was calibrated by polystyrene standards (M_w: 2500−900000 g/mol) and was controlled through Breeze software. Tetrahydrofuran was used as the mobile phase at a flow rate of 1.0 mL/min at 313 K. Composition of the copolymer was determined by ^{1}H NMR spectroscopy in $CDCl_3$ at 303 K, using a Bruker AC 300 instrument.

Salt Doping. A 5w/v % solution of the diblock copolymers was initially prepared in tetrahydrofuran. Subsequently, it was separated to four solutions in which weighted amounts of LiTf or of EMITf were added to form [EO]:[LiTf] or [EO]:[EMITf] doping rations of 8:1, 4:1, and 2:1. The resulted block copolymer electrolytes were isolated by evaporation of the solvent and dried to a constant weight under vacuum. The preparation route for salt incorporation is shown in Scheme 1. The molecular characteristics of the initial diblock copolymers and composition data for the corresponding block copolymer electrolytes are summarized in Table 1. It is noted that in all cases the volume fractions were calculated as

Scheme 1. Reaction Scheme Leading to the Preparation of the Block Copolymer Electrolytes

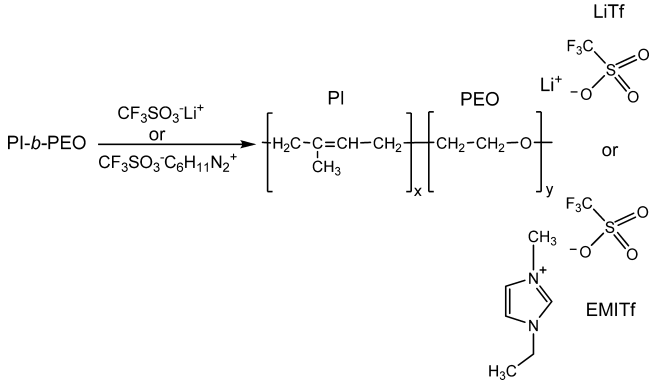

DOI: 10.1021/acs.macromol.5b00089
Macromolecules 2015, 48, 1473−1482

Table 1. Molecular Characteristics of the Poly(isoprene)-*b*-poly(ethylene oxide) Block Copolymer Electrolytes

sample	[EO]:[salt]	w_{PEO} (wt %)	w_{PI} (wt %)	f_{PI}
$IEO_{307-204}$[a]	–	30.0	70.0	0.74
$IEO_{307-204}$/LiTf-8	8:1	26.5	61.8	0.72
$IEO_{307-204}$/LiTf-4	4:1	23.7	55.3	0.69
$IEO_{307-204}$/LiTf-2	2:1	19.6	45.7	0.62
$IEO_{307-204}$/EMITf-8	8:1	24.6	57.3	0.64
$IEO_{307-204}$/EMITf-4	4:1	20.8	48.5	0.57
$IEO_{307-204}$/EMITf-2	2:1	15.9	37.1	0.46
$IEO_{111-201}$[a]	–	54	46	0.51
$IEO_{111-201}$/LiTf-8	8:1	43.6	37.1	0.48
$IEO_{111-201}$/LiTf-4	4:1	36.5	31.1	0.44
$IEO_{111-201}$/LiTf-2	2:1	27.6	23.5	0.37
$IEO_{111-201}$/EMITf-8	8:1	38.6	32.9	0.39
$IEO_{111-201}$/EMITf-4	4:1	30	25.6	0.32
$IEO_{111-201}$/EMITf-2	2:1	20.8	17.7	0.27

[a]The weight-averaged molecular weight of $IEO_{307-204}$ is M_w = 29900 g/mol, the polydispersity index M_w/M_n = 1.03 and the degrees of polymerization of the PI and PEO blocks are indicated as x/y = 307/204. The molecular weight of $IEO_{111-201}$ is 16400 g/mol.

$$f_{PEO,PEO-LiTf,PEO-EMITf} = \left[1 + \left(\frac{1}{w_{PEO,PEO-LiTf,PEO-EMITf}} - 1\right)\frac{\rho_{PEO,PEO-LiTf,PEO-EMITf}}{\rho_{PI}}\right]^{-1} \quad (1)$$

where ρ_{PEO} = 1.13 g/cm^3[38] and ρ_{PI} = 0.92 g/cm^3,[38] while $\rho_{PEO\text{-}LiTf}$ and $\rho_{PEO\text{-}EMITf}$ at each ratio are calculated based on

$$\rho_{PEO-LiTf,PEO-EMITf} = \frac{w_{PEO}\rho_{PEO} + w_{LiTf,EMITf}\rho_{LiTf,EMITf}}{w_{PEO-LiTf,PEO-EMITf}} \quad (2)$$

where ρ_{LiTf} = 2.135 g/cm^3,[39] and ρ_{EMITf} = 1.387 g/cm^3.[40]

2.2. Characterization Methods. *Differential Scanning Calorimetry (DSC).* A Q2000 (TA Instruments) was used for thermal analysis with a cooling/heating rate of 10 K/min at a temperature range from 153 to 473 K. The instrument was calibrated for best performance on the specific temperature range and heating/cooling rate. The calibration sequence included a baseline calibration for the determination of the time constants and capacitances of the sample and reference sensor using a sapphire standard, an enthalpy and temperature calibration for the correction of thermal resistance using indium as standard (ΔH = 28.71 J/g, T_m = 428.8 K), and a heat capacity calibration with sapphire standard.

X-ray Scattering. Both wide-angle and small-angle X-ray scattering (WAXS/SAXS) measurements were made from macroscopically oriented filaments with a diameter of 1.0 mm. For the SAXS measurements an 18 kW rotating anode X-ray source (Rigaku) was used with a pinhole collimation and a two-dimensional (2D) detector (Bruker) with 1024 × 1024 pixels. A double graphite monochromator for the CuKα radiation (wavelength λ = 0.154 nm) was used, and the sample-to-detector distance was set at 1.8 m. The WAXS measurements were made using a pinhole collimator and a two-dimensional detector (Bruker) with 1024 × 1024 pixels. A graphite monochromator was used (λ = 0.154 nm), and the sample-to-detector distance was 7.5 cm. In both experiments (SAXS/WAXS) 2D images were recorded and the 2D scattered intensity distributions were investigated over the azimuthal angle and are presented as a function of the scattering wave vector q ($q = (4\pi/\lambda)\sin(2\theta/2)$, where 2θ is the scattering angle). X-ray measurements were made on heating at temperatures in the range from 303 to 393 K in steps of 10 K and on subsequent cooling. One hour long measurements were taken at each temperature with stability better than ±0.2 K. Representative scattering curves for the $IEO_{111-201}$/LiTf at 4:1 [EO]:[LiTf] ratio as a function of temperature are depicted in Figure S1, Supporting Information.

FTIR Spectroscopy. Spectra in the mid-infrared region were measured on a Fourier transform spectrometer (Equinox 55, Bruker Optics) equipped with a single reflection diamond attenuated total reflectance (ATR) accessory (DuraSamplIR II, SENSIR). The spectra were measured over the 525−5000 cm^{-1} range at a resolution of 2 cm^{-1} and represent averages of 100 scans. ATR spectra were measured directly on samples, which were brought in contact with the diamond element using a torque press accessory.

Dielectric Spectroscopy (DS). All samples were prepared in a glovebox under controlled nitrogen atmosphere (oxygen and water content of less than 0.1 ppm) to avoid oxidation and water intake. Samples were first heated within the glovebox at the melting temperature of the complex. During heating samples acquired an amber color. Then samples were deposited on the electrodes and slightly pressed in order to uniformly spread between the electrodes and optimize the contact. Three different electrode materials were used: brass, stainless steel and Au-coated electrodes. The sample capacitors consisted of two electrodes 20 mm in diameter and the sample thickness, maintained by Teflon spacers, was in the range of 40−60 μm. Dielectric measurements were performed at atmospheric pressure in the temperature range from 133 to 453 K. Typically, four heating/cooling cycles were employed to ensure reproducibility and to monitor possible sample degradation.

The DS measurements were made in the frequency range from 1 × 10^{-2} to 1 × 10^6 Hz, using a Novocontrol BDS system composed of a frequency response analyzer (Solartron Schlumberger FRA 1260) and a broadband dielectric converter. Conductivity studies were made using the analysis of the complex conductivity function through $\sigma^* = \sigma' + i\sigma''$, which is related to the complex dielectric permittivity with $\sigma^* = i\omega\varepsilon_0\varepsilon^*$.[41,42] To obtain the dc-conductivity, two methods were employed. First, we employed the random free-energy barrier model by Dyre.[43] The model assumes that conduction takes place by hopping, where the hopping charge carriers are subject to spatially randomly varying energy barriers. According to the model, the onset of dc-conductivity is determined by crossing the highest energy barrier. The model, solved in the continuous time random walk approximation, provides an analytical expression for the complex dielectric function as[41,43] $\varepsilon^*(\omega) = \varepsilon_\infty + \sigma_0\tau_e/[\varepsilon_0 \ln(1 + i\omega\tau_e)]$, where ε_∞ is the value of ε' in the limit of high frequencies and σ_0, τ_e are the dc-conductivity and characteristic time of ion motion. The model predictions are tested earlier against the experimental data at three temperatures for the $(PEO)_4LiCF_3SO_3$ compound. The predictions can only partially fit the experimental data and within a limited frequency range. We attribute these deviations to the nature of polymer electrolyte. The present system cannot be considered as disordered and, in addition, formation of the complex is strongly temperature-dependent. Second, the dc-conductivity can be obtained by the plateau in the real part, σ' without invoking any model.

3. RESULTS AND DISCUSSION

3.1. Thermal Properties. DSC traces of the block copolymer electrolytes containing LiTf salt and EMITf ionic liquid are shown in Figures 1 and 2 for the low and high molecular weight block copolymers, respectively. At high salt concentration (i.e., [EO]:[Li^+] = 4:1 and [EO]:[Li^+] = 2:1) incorporation of LiTf (Figure 1a) in $IEO_{111-201}$ suppresses PEO crystallization, while at the low salt concentration, i.e. [EO]:[Li^+] = 8:1, PEO can crystallize but with a lower degree of crystallinity (Table 2). This suggests that the ether oxygens of the PEO block form transient cross-links with Li^+ ions of the salt that inhibit PEO crystallization depending on the salt concentration. The existence of a second melting endotherm observed above 393 K, signifies the presence of $(PEO)_3LiTf$ crystalline compound (complex).[6−8] This behavior is reminiscent of PEO/LiTf electrolytes studied earlier by some of us.[8] The corresponding traces are depicted by the dashed lines in

DOI: 10.1021/acs.macromol.5b00089
Macromolecules 2015, 48, 1473−1482

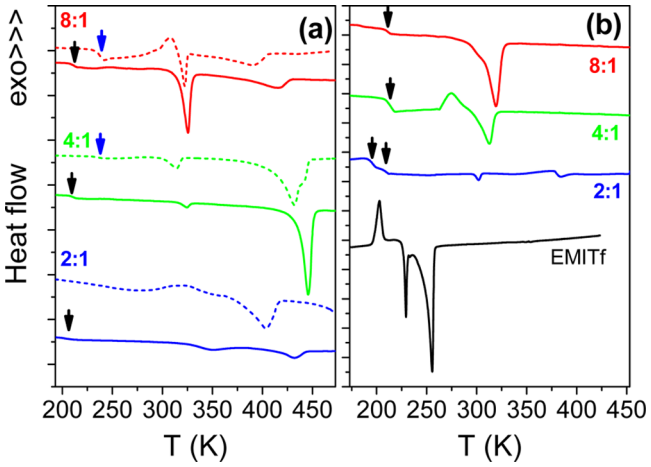

Figure 1. DSC thermograms of the $IEO_{111-201}$ block copolymer electrolytes based on (a) LiTf and (b) EMITf at different salt concentrations: [EO]:[salt] = 8:1 (red), 4:1 (green). and 2:1 (blue). The dashed lines in part a give the corresponding thermograms for the PEO/LiTf electrolytes. In part b, the pure ionic liquid is presented with the black line. Arrows indicate glass temperatures. Traces are shifted vertically for clarity.

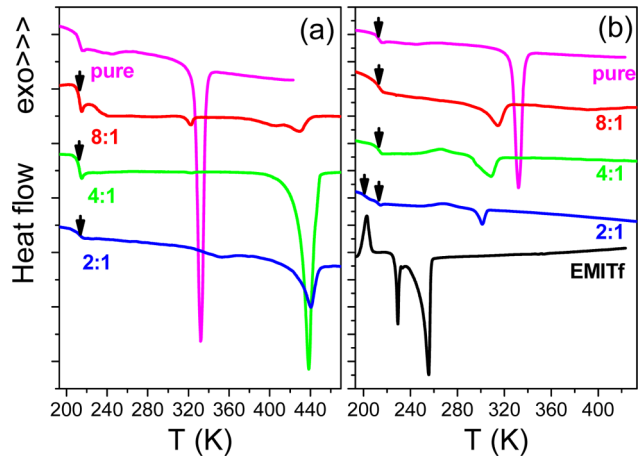

Figure 2. DSC thermograms of the $IEO_{307-204}$ block copolymer electrolytes based on (a) LiTf and (b) EMITf at different salt concentrations: [EO]:[salt] = 8:1 (red), 4:1 (green), and 2:1 (blue). The thermogram of pure block copolymer in part a is presented with the magenta line, while the pure ionic liquid in part b is shown with the black line. Arrows indicate glass temperatures. Traces are shifted vertically for clarity.

Figure 1a for comparison.[8] Two endothermic peaks, one at ~323 K and one above 373 K, corresponding to PEO crystal and complex crystal melting, respectively, where found. The former peak had a decreasing heat of fusion, ΔH, while the latter increasing heat of fusion with increasing salt concentration, denoting the gradual complexation of Li ions to ether oxygens that suppress PEO crystallization (Table 2). The blue arrows in the same figure signify a step-like change of the heat flow at the glass temperature (T_g) of PEO/LiTf electrolytes. This step is shifted to higher temperatures with respect to the PEO homopolymers due to the formation of cross-links between Li^+ and ether oxygen atoms. This, in effect, makes the Li^+-complexed PEO a polyelectrolyte, as has been suggested by recent self-consistent field theory.[20−22]

In the block copolymer electrolytes, a similar step cannot be clearly discerned in the DSC traces. Instead, a glass temperature is found at ~213 K (black arrows) corresponding to the freezing of PI segmental motion.

The incorporation of the bulkier IL in the PEO phase has drastically different effects, as shown in Figure 1b. Only one endothermic peak is observed at all [EO]:[EMITf] ratios corresponding to the melting of PEO crystals. Increasing EMITf concentration results in a decrease in the melting temperature and, in addition, to a suppressed PEO crystallinity.[44,45] Similar effects were observed when EMITf was dissolved in other polymeric matrices such as in poly(vinylidene fluoride-*co*-hexafluoropropylene) (PVDF-HPF)[46] and are attributed to the plasticizing role of EMITf. A glass temperature corresponding to PI is indicated by black arrows in Figure 1b at ~213 K, independent of the ionic liquid concentration. At the highest concentration employed, [EO]:[EMITf] = 2:1, a second glass temperature is observed at 200 K, i.e., the T_g of plasticized PEO. Pure EMITf has a T_g at 172 K, a crystallization peak at 200 K and two melting peaks at 229 K and at 256 K.[28]

For the higher molecular weight diblock copolymer, $IEO_{307-204}$, (Figure 2) an endothermic peak is detected at 332 K, corresponding to the melting of PEO crystals. The calculated PEO degree of crystallinity in the neat diblock is X_c = 0.77 (based on the heat of fusion of 100% crystallized PEO, ΔH_∞ = 196 J/g) (Table 2).[47] As with the lower molecular weight block copolymer, incorporation of LiTf (Figure 2a) in the PEO phase nearly completely suppresses the PEO crystallinity, as indicated by the absence of an endothermic peak within the 313−333 K region for all [EO]:[LiTf] ratios. The existence of $(PEO)_3$LiTf crystalline compound is also evident from the second melting endotherm above 393 K at all compositions. Figure 2b shows the effect of IL incorporation, which is more pronounced than in the $IEO_{111-201}$ case. Here, there is a decrease in the PEO melting temperature and a suppressed PEO crystallization. With respect to the glass temperature, indicated by arrows, in all $IEO_{307-204}$ electrolytes there is a single T_g ~213 K, originating from the PI block with the exception of the 2:1 IL case where a second step is seen at 200 K reflecting the plasticized PEO.

In short, the effect of incorporation of LiTf in the thermodynamic properties of both IEO copolymers is reminiscent of the PEO/LiTf electrolytes studied earlier. There is an interplay between two ordered structures, the PEO crystals and the crystalline complex, and their relative contribution depends strongly on LiTf content. On the other hand, incorporation of EMITf does not induce complexation indicating a weaker interaction between PEO and EMI^+ ions. More precise information on ion association can be obtained by IR (below). Nevertheless, these fundamental structural and thermodynamic differences between the LiTf and the IL are expected to have consequences in ion transport.

3.2. Ion Local Environment and Ion Association. Ion association was studied by infrared (IR) spectroscopy. This technique is a convenient and powerful tool for probing both ion−polymer interactions and ionic association effects. Infrared spectra of the high molecular weight diblock copolymer $IEO_{307-204}$ and its block copolymer electrolytes are depicted in Figure 3. Dissolution of the triflate salt in the PEO phase is expected to affect the C−O−C vibrations of the PEO backbone (where oxygen atoms of the ether group are involved in the coordination environment of cations). Hence, probing

DOI: 10.1021/acs.macromol.5b00089
Macromolecules 2015, 48, 1473−1482

Table 2. Melting Temperatures of PEO Crystals and of the Complex Crystal ($(PEO)_3LiTf$) and Corresponding Degrees of Crystallinity for All Studied Block Copolymer Electrolytes

	T_m^{PEO} (K)	X_c^{PEO} (%)	$T_m^{complex}$ (K)	$X_c^{complex}$ (%)
$IEO_{307-204}$	59	76.9	–	–
$IEO_{111-201}$/LiTf 8:1	325	31	415	18
$IEO_{111-201}$/LiTf 4:1	324	3	445	54
$IEO_{111-201}$/LiTf 2:1	–	–	431	9
$IEO_{111-201}$/EMITf 8:1	318	50	–	–
$IEO_{111-201}$/EMITf 4:1	312	28	–	–
$IEO_{111-201}$/EMITf 2:1	302	3	--	–
$IEO_{307-204}$/LiTf 8:1	322	2	430	23
$IEO_{307-204}$/LiTf 4:1	–	–	438	97
$IEO_{307-204}$/LiTf 2:1	–	–	440	23
$IEO_{307-204}$/EMITf 8:1	314	30	–	–
$IEO_{307-204}$/EMITf 4:1	308	30	–	–
$IEO_{307-204}$/EMITf 2:1	311	12	--	–

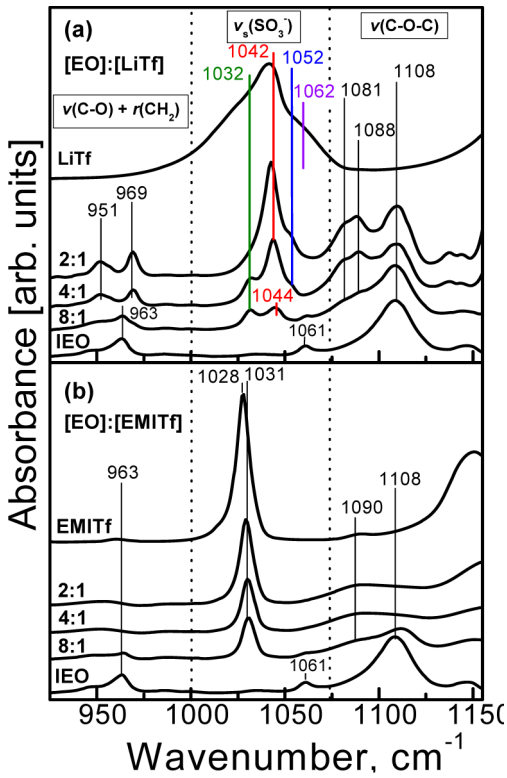

Figure 3. IR absorption spectra of the high molecular weight diblock copolymer $IEO_{307-204}$ and of the block copolymer electrolytes with (a) LiTf and (b) EMITf, at three [EO]:[salt] ratios at T = 293 K. The spectra are scaled on the 1375 cm^{-1} band (not shown) and offset to facilitate comparison.

vibrations of the triflate group can be employed as a fingerprint of the local structure in the ionic domains of the block copolymer.

$IEO_{307-204}$ exhibits a strong band at 1108 cm^{-1} arising from the ν(C−O−C) vibration of noncoordinated ether oxygen atoms. As observed in Figure 3a, absorption in this region changes progressively as LiTf is introduced in the PEO domain. Most pronounced is the decrease of relative intensity at ca. 1108 cm^{-1} while new bands develop at ca. 1081 and 1088 cm^{-1} with increasing salt content. These bands originate from the participation of PEO ether oxygens in the coordination sphere of lithium ions.[48] The remaining intensity at 1108 cm^{-1} gives the fraction of noncoordinated ether oxygens with Li^+.

The 963 cm^{-1} band of $IEO_{307-204}$, originating from the ν(C−O) + $r(CH_2)$ vibration in crystalline PEO,[49] is also affected by the addition of LiTf, with a broadening and eventually splitting to two new bands at 951 and 969 cm^{-1}. These bands are attributed to ν(C−O) + $r(CH_2)$ in the crystalline complex, as they were absent following melting of the stoichiometric complex.[50]

The $\nu_s(SO_3^-)$ mode is found to give rise to different peaks in the spectral region 1000−1070 cm^{-1}. As this mode is nondegenerate (A_1 symmetry) the observed multiple peaks for $\nu_s(SO_3^-)$ indicate the presence of triflate anions in different potential energy environments. At the lowest LiTf concentration, two bands appear at 1032 and 1044 cm^{-1} (Figure 3a), that are assigned to free triflate anions[50,51] and contact ion pairs, respectively. With increasing salt content, the band at 1042 cm^{-1} provides the most intense contribution in this spectral range, originating from contact ion pairs. Furthermore, a third component at 1052 cm^{-1} can be clearly discerned as a shoulder corresponding to higher ion complexes $(Li_2Tf)^+$.

It can be observed that at low salt concentrations a significant proportion of triflate ions are "free" (Figure S3, Supporting Information), while increasing LiTf content favors ion pairing effects. Figure 3a suggests that more complexed species are formed at higher salt concentrations, involving different types of aggregates of triflate anions with lithium cations. We should mention here that higher ion complexes where not considered by a recent self-consistent field-theory for salt-doped diblock copolymers based on PEO.[20−22] In addition, the fraction of ion pairs for a composition of [EO]:[LiTf] ∼ 10:1 was underestimated. The expectation is that the different types of ionic species make their own contribution to the ionic conductivity, e.g., the formation of contact ion pairs would decrease the number of mobile charge carriers and, therefore, reduce ionic conductivity as compared to the "free" ion case (see below).

On the other hand, incorporation of EMITf has remarkably different effects as seen in Figure 3b. The intensity of the ν(C−O−C) band of $IEO_{307-204}$ at ca. 1108 cm^{-1} is decreasing upon EMITf incorporation in the PEO phase suggesting a weak interaction with EMI^+.[25] The same trend is found also with the 963 cm^{-1} band. Since the latter feature is attributed to the ν(C−O) + $r(CH_2)$ vibration of crystalline PEO, its suppressed intensity suggests a reduced PEO crystallinity in agreement with the DSC results (Figures 1 and 2).

A pronounced difference between EMITf and LiTf is observed also in the $\nu_s(SO_3^-)$ spectral region. At the lowest

DOI: 10.1021/acs.macromol.5b00089
Macromolecules 2015, 48, 1473−1482

ionic liquid concentration a single band appears at 1031 cm^{-1}, that is also found in pure EMITf (Figure 3b). At higher EMITf content the band gains intensity and shifts eventually to 1028 cm^{-1}. In addition, the emergence of a single band in this spectral region indicates that the sulfonic group of the triflate anion vibrates in a single potential energy environment, i.e., the triflate anion remains uncoordinated or "free". The slight shift of $\nu_s(SO_3^-)$ vibration (from 1028 cm^{-1} in IEO/EMITf to 1032 cm^{-1} in IEO/LiTf) suggests a similar -but not identical- "free" triflate anion environment in the two systems. Such differences in local packing result from the different interactions of LiTf and EMITf with PEO phase, and are expected to significantly affect the dc conductivity of the corresponding electrolyte systems (see below).

3.3. Local and Global Structure. The coordination of Li ions with ether oxygens leads to the formation of a complex crystal who's local structure is well-known.[7,8] Figure 4 provides

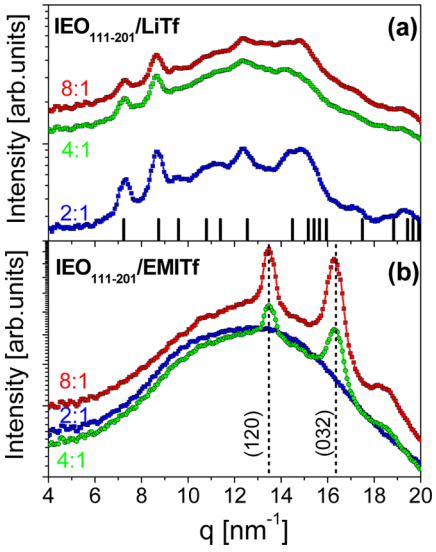

Figure 4. Wide angle X-ray scattering from the low molecular weight $IEO_{111-201}$ enriched in (a) LiTf and (b) EMITf at three salt concentrations as indicated at 293 K. The dashed vertical lines in part b correspond to the (120) and (032) reflections from the monoclinic unit cell of PEO. The short vertical lines in part a correspond to the main reflections of the complex crystal with the stoichiometric composition $(PEG)_3LiTf$.

with the WAXS spectra of the low molecular weight copolymer $IEO_{111-201}$ containing either (a) LiTf or (b) EMITf at various concentrations. Complexation of Li ions with PEO is evident in Figure 4a from the absence of PEO crystallization and the presence of new reflections -depicted by black vertical lines- corresponding to the crystalline complex. The latter has a monoclinic unit cell with lattice parameters a = 1.6768 nm, b = 0.8613 nm, c = 1.007 nm, and β = 121.02°. In contrast to this, the weak interactions of EMITf with PEO prevent the formation of a crystalline complex. Both ions are uncoordinated or "free" and this is expected to increase ionic conductivity (see below). As a consequence, PEO is now able to crystallize, in agreement with DSC and IR results. It does so in the usual monoclinic unit cell with lattice parameters a = 0.805 nm, b = 1.304 nm, c = 1.948 nm, and β = 125.04°.[52]

SAXS measurements were performed to explore the effect of LiTf and IL incorporation on the diblock copolymer phase state and the corresponding periodicity. Figure 5 provides

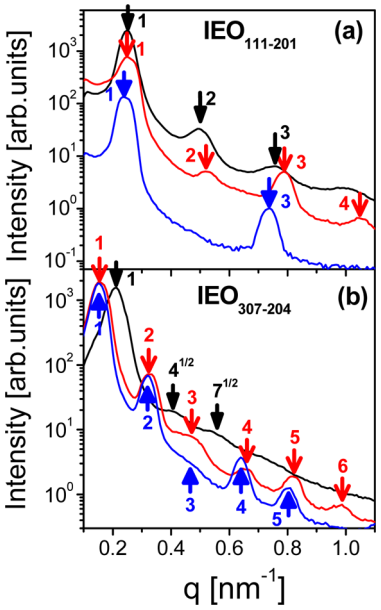

Figure 5. SAXS spectra of bulk IEO (black lines), and their electrolytes with [EO]:[LiTf] = 8:1 (red lines) and [EO]:[EMITf] = 8:1 (blue lines) for (a) the low molecular weight $IEO_{111-201}$ and (b) the high molecular weight $IEO_{307-204}$. All data refer to 293 K.

representative scattering curves at 293 K for block copolymers $IEO_{111-201}$, $IEO_{307-204}$, and the corresponding electrolytes bearing the same salt content, $[EO]:[Li^+] = [EO]:[EMI^+]$ = 8:1. The phase diagram of PI-*b*-PEO diblock copolymers is well documented in literature.[34,35] In the symmetric $IEO_{111-201}$, diffraction peaks appear at relative positions 1:2:3 revealing a lamellar nanostructure (Figure 5a). In the asymmetric $IEO_{307-204}$ (f_{PI} = 0.70), the scattering pattern consists of a maximum at a wave vector of 0.21 nm^{-1} and higher order features at approximate positions $1:4^{1/2}:7^{1/2}$ relative to the main peak (Figure 5b). Assuming cylinders in a hexagonal lattice, the higher order peaks should appear at relative positions $1:3^{1/2}:4^{1/2}:7^{1/2}:9^{1/2}$. The absence of this sequence of reflections suggests a hexagonal lattice in the absence of long-range order.

Incorporation of LiTf or EMITf within the PEO phase of $IEO_{307-204}$ has two effects on the SAXS pattern; first, the main peak at q^* shifts to lower q values, and, second, higher order peaks appear at relative positions 1:2:3:4:5:6. The former effect reveals enhanced unfavorable interactions between the blocks and/or swelling,[53−55] whereas the latter suggests the formation of lamellar nanodomain morphology with long-range order. Increasing volume fraction, induced by lithium salt incorporation cannot solely account for the full change in the domain spacing. An increase in domain spacing, d, is associated with an increase in the effective interaction parameter, χ_{eff} that characterizes the unfavorable interactions between unlike blocks and this can have different origins. In one picture, coordinated Li ions to ether oxygens stiffen the PEO backbone and induce a change in nanodomain structure toward more segregated domains. In this view, χ_{eff} can be obtained from the nanodomain spacing by assuming the same dependence on the product χN as in strongly segregated block copolymers (strong segregation limit (SSL)), *i.e.*, $d \sim \chi_{eff}^{1/6} N^{2/3}$.[5] This naturally results in a higher χ_{eff} and to a narrower interfacial width with increasing salt concentration.

A more recent self-consistent field theory[20−22] provided a very different view as to the origin of increasing domain spacing

DOI: 10.1021/acs.macromol.5b00089
Macromolecules 2015, 48, 1473−1482

in salt-doped block copolymers. The theory is based on the observation that salt doping induces changes not only in the ordered phases of block copolymers but also in the disordered phase. The disordered phase structure factor of doped block copolymers is fundamentally different from the one in pure diblock copolymers. In bulk block copolymers the structure factor peak originates from the correlation hole effect, *i.e.*, the fact that even in the disordered phase there exist concentration fluctuations of a "fixed" length scale corresponding to the mean-distance between blocks. In doped block copolymers this peak is shifted to larger wavenumbers suggesting a smaller length scale for phase separation. The implication of this is that the *d*-spacing contains additional contributions suggesting that a more accurate way of obtaining χ_{eff} is from the shift of the spinodal of the disordered phase. It is argued[21] that this shift provides a more fundamental measure of the increasing effective repulsion in the doped block copolymers. Furthermore, the theory employed an expression for the solvation energy in the form of the local Born model and a mixing rule for the dielectric permittivity of the effective "medium". The preferential solvation energy of the anions was found to be the key point for the increasing nanophase separation. The tendency for the anions to be preferentially solvated by one of the blocks results in an effective repulsion between the blocks which in turn leads to increased domain spacing. The theory predicts a linear increase of the interaction parameter with increasing molar ratio, *r*, of Li ions to EO monomers, as $\chi_{\text{eff}} = \chi + mr$, where χ is the intrinsic interaction parameter of the bare block copolymer and *m* is a function of the anion size. In the limit of complete ion dissociation linearity prevails, whereas a nonlinear dependence is predicted in the presence of strong ion-pairing as observed experimentally (Figure 3).

Ideally, the effective interaction parameter can be obtained from the disordered phase structure factor. However, this is impossible in the present case as the IEO/LiTf system remains in the nanophase separated state up to the highest temperature investigated (SSL) (Figure S1, Supporting Information). This is reflected in the strong temperature dependence of the bare interaction parameter, $\chi = 65/T + 0.125$.[34,35] For this reason the model predictions on χ_{eff} cannot be tested. In this case, χ_{eff} can be extracted either by assuming linearity ($d \sim \chi_{\text{eff}}^{1/6} N^{2/3}$) or by employing the same dependence for $\chi_{\text{eff}}(N,r)$ as in the PS–PEO/LiTFSI system studied earlier.[18] Clearly, the two approaches lead to a very different χ_{eff} and hence to a different interfacial width. An argument in favor for the latter approach in extracting χ_{eff} is the presence of strong ion-pairing that, furthermore, is a function of salt content (Figure 3 and Figure S3, Supporting Information).

Independent of the origin of increasing domain spacing we can compare the effect of different salt doping on the domain spacing. Figure 6 depicts the domain spacing in the IEO/LiTf and IEO/EMITf systems for both copolymers. Despite the different dependence of the domain spacing for the high and low molecular weight copolymers (this is only partially due to the hexagonal-to-lamellar phase transformation in the higher molecular weight block copolymer), the dependence of *d* for LiTf and the IL is very similar. This is due to different effects; in the case of LiTf the increase in domain spacing reflects the increase on the effective interaction parameter due to cation complexation and anion solvation effects whereas in the IL case due to swelling. Hence these systems provide the possibility of studying ion transport under identical domain spacing conditions but with different interactions/local structures.

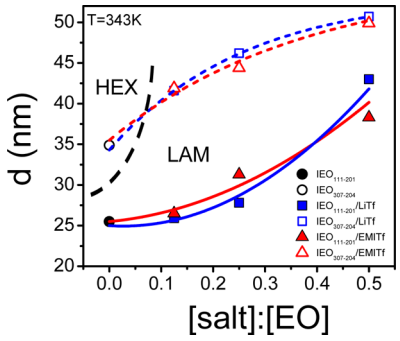

Figure 6. Domain spacing plotted as a function of salt concentration for $IEO_{307-204}$ (empty symbols, dashed lines) and $IEO_{111-201}$ (filled symbols, solid lines). All data correspond to 343 K.

3.4. dc-Conductivity. The dc-conductivities in the IEO/LiTf electrolytes are discussed in view of recent measurements in the corresponding PEO/LiTf electrolytes made on identical temperatures and salt concentrations.[8] In the latter system, the temperature dependence of dc-conductivity was found to reflect the continuous structural changes (melting of PEO crystals and continuous melting of crystalline complex). These structural changes were held responsible for the departure from the usual Vogel–Fulcher–Tammann (VFT) or Arrhenius dependencies. It was further shown[8] that ion transport is dominated by (i) the amorphous phase that is enriched with LiTf ions, and to a smaller extent by (ii) the stoichiometric complex itself. It was suggested that ion transport requires the continuous supply of ions from the ion sink following the continuous melting of the crystalline complex and melted PEO domains where ions are incorporated and transported.

The dc conductivities in the low molecular weight $IEO_{111-201}$/LiTf electrolytes with [EO]:[LiTf] = 4:1 and [EO]:[LiTf] = 8:1 are shown in Figure 7a as a function of temperature. Evidently, the *T*-dependence of dc-conductivity is neither VFT nor Arrhenius as with the parent PEO/LiTf electrolytes. This reflects the continuous melting of crystalline complex starting already from temperatures above the melting of PEO crystals (Figures 1 and 2). Both features are evident in the $\sigma(T)$ dependence of the electrolyte with [EO]:[LiTf] = 8:1, whereas only the former feature in the electrolyte with [EO]:[LiTf] = 4:1 due to the suppressed crystallinity. As with the parent PEO/LiTf system, the dc-conductivity in the $IEO_{111-201}$/LiTf is higher at the lower salt content. This reflects the high dissociation of LiTf found in IR (Figure 3 and Figure S3 Supporting Information), and the increased concentration of free charge carriers. In particular, the maximum in σ_{dc} occurs at the same LiTf content corresponding to the maximum content of free ions (Figure 7b). At a higher LiTf content, *i.e.*, [EO]:[Li] = 4:1, σ_{dc} decreases drastically and this is attributed to additional ion-pair formation and to the highly crystalline complex crystal that dominates the local structure.

On the other hand, the dc-conductivity in the $IEO_{111-201}$/EMITf system is drastically different. First, conductivities are some orders of magnitude higher as compared to the LiTf case. Second, they show an opposite dependence on electrolyte content increasing with EMITf content. Third, $\sigma(T)$, shows a VFT *T*-dependence above and below the melting of PEO crystals. This situation in the two systems is depicted Figure 7b. The comparison is made at a temperature just above the melting of crystalline complex, for the LiTf electrolytes, and at a

DOI: 10.1021/acs.macromol.5b00089
Macromolecules 2015, 48, 1473–1482

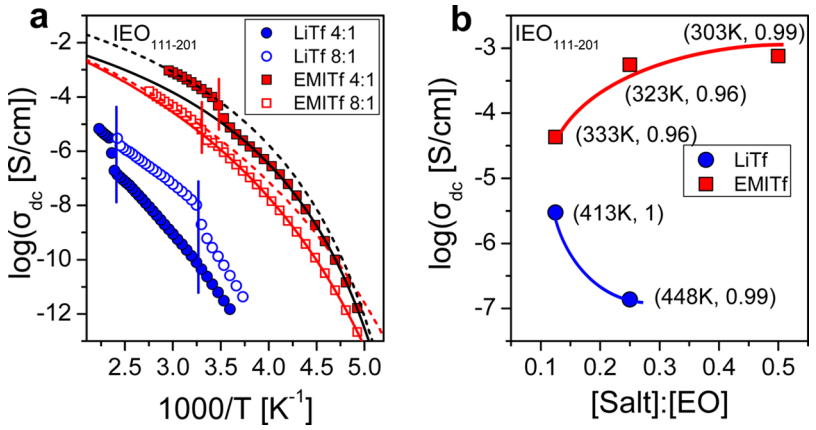

Figure 7. (a) Dc-conductivities for the $IEO_{111-201}$ block copolymer electrolytes with [EO]:[LiTf] = 4:1 (blue filled circles), [EO]:[LiTf] = 8:1 (blue open circles), [EO]:[EMITf] = 4:1 (red filled squares), and [EO]:[EMITf] = 8:1 (red open squares). The red curves, solid and dashed, represent VFT fits to the [EO]:[EMITf] = 8:1 composition at temperatures below and above the melting of PEO, respectively. Black lines, solid and dashed, represent VFT fits to the [EO]:[EMITf] = 4:1 composition at temperatures below and above the melting of PEO, respectively. Vertical blue lines indicate PEO crystal melting (at 3.25) and complex crystal melting (at 2.5) of the LiTf containing electrolytes. Vertical red lines indicate PEO crystal melting in the EMITf containing electrolytes. (b) Dc-conductivities compared at the melting of complex crystals for the LiTf electrolytes and just above the melting of PEO crystals for the EMITf electrolytes. Numbers in parentheses indicate the actual temperatures as well as the reduced temperatures with respect to the melting of PEO crystals (IEO/EMITf) and to the melting of the crystalline complex (IEO/LiTf).

temperature just above the melting of PEO crystals for the EMITf electrolytes. Despite the lower temperature for the EMITf, conductivities are some orders of magnitude higher especially at the higher salt concentrations. Obviously, ion transport in the two cases is fundamentally different. In IEO/EMITf, ions are fully dissociated as shown by IR. Furthermore, EMITf has a plasticizing role on the segmental dynamics of PEO. Both effects lead to increasing ion conductivity in IEO/EMITf. The dc-conductivities in the $IEO_{111-201}$/EMITf case are compared with the parent PEO/EMITf electrolyte in Figure S4, Supporting Information. The figure depicts conductivity measurements of bulk EMITf obtained by fast cooling—to avoid crystallization—and subsequent heating, as well as, by slow cooling before the onset of crystallization. The $\sigma(T)$ dependence of bulk EMITf can be fitted according to the VFT dependence as

$$\sigma = \sigma_0 \exp\left(\frac{B}{T - T_0}\right) \quad (3)$$

where $\sigma_0 \sim 13$ S/cm, with an activation parameter B (=1230 K) and an "ideal" glass temperature of $T_0 = 127$ K. Conductivities in the $IEO_{111-201}$/EMITf with [EO]:[EMITf] = 4:1 and [EO]:[EMITf] = 8:1 were very similar to the corresponding PEO/EMITf cases. The activation parameter and "ideal" glass temperature for the $IEO_{111-201}$/EMITf 4:1 are 1280 ± 67 K and 150 ± 2 K, respectively. The activation parameter and "ideal" glass temperature for the $IEO_{111-201}$/EMITf 8:1 are 2050 ± 25 K and 130 ± 1 K, respectively. Moreover, conductivity values of ∼1 mS/cm were obtained at ambient temperature for $IEO_{111-201}$/EMITf 4:1 composition, a value typical of several ILs but in our case in the presence of an elastic, solid-like, response.[24]

More information on the effect of local structure/interactions on the ionic conductivity can be obtained by comparing with independent measurements made on the corresponding homopolymer electrolytes. The comparison of the conductivities in $IEO_{111-201}$/LiTf and $IEO_{111-201}$/EMITf electrolytes to the corresponding homopolymer electrolytes, PEO/LiTf and PEO/EMITf, is made in Figure 8. Conductivity is now

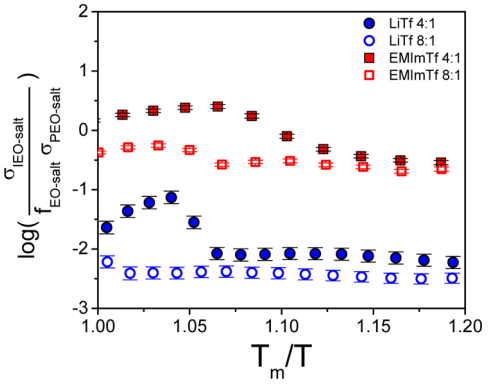

Figure 8. Normalized conductivities of $IEO_{111-201}$ with [EO]:[LiTf] = 4:1 (blue filled circles), [EO]:[LiTf] = 8:1 (blue open circles), [EO]:[EMITf] = 4:1 (red filled squares) and [EO]:[EMITf] = 8:1 (red open squares). The horizontal axis is the normalized temperature with respect either to the melting temperature (T_m) of complex (LiTf) or to the melting of crystalline PEO (EMITf).

expressed as the ratio of the diblock copolymer electrolyte conductivity over that of the homopolymer electrolyte corrected for the volume fraction of the salt containing PEO phase ($f_{EO\text{-}salt}$). We emphasize here that the neat electrolyte measurements are made separately under identical conditions and for the same compositions. In the EMITf electrolytes the normalized conductivity is near unity suggesting the absence of any contribution from the block copolymer periodic nanostructure. In contrast to this, in LiTf electrolytes there is a decrease of conductivity by one to 2 orders of magnitude relative to the PEO/LiTf case. We mention here that a decreasing relative conductivity has also been reported in PS–PEO (SEO)/LiTFSI electrolytes.[17] In the limit of high molecular weights (M_{SEO} > 100 kg/mol) a reduction to a value of 2/3 has been reported which corresponds to the maximum conductivity for randomly oriented lamellar grains.[17] Additional conductivity reduction effects were seen for low and intermediate molecular weights originating from the glass temperature of the nonconducting phase (PS in their case) and

DOI: 10.1021/acs.macromol.5b00089
Macromolecules 2015, 48, 1473−1482

the width of the doped phase, respectively. For a SEO with M_w ~ 10 kg/mol, the reduction was more than an order of magnitude (a factor of 25 was reported).[17] In the present case, the reduction is even higher (a factor of ~100 for [EO]:[Li] of [8]:[1]). Several factors can result in such reduction (induced defects, grain size, etc.). Here we explore the different wetting properties of the two nanophases, *i.e.*, PI and PEO/LiTf, on the electrodes used in the DS study. Contact angle measurements performed at ambient temperature (PI) and at 458 K (PEO/LiTf), the latter corresponding to the melt state, revealed preferential wetting of the electrodes by PEO/LiTf independent of the electrode material used in DS (Figure S5, Supporting Information). Preferential wetting of one of the electrodes may result is several layers of PEO/LiTf having a blocking orientation, i.e., with the lamellar normal perpendicular to the electrode surface. This effect can lead to a further reduction in the normalized conductivity as observed experimentally.

4. CONCLUSION

The incorporation of the archetypal electrolyte LiTf and of the ionic liquid EMITf—bearing the same anion but different cations—to strongly incompatible IEO diblock copolymers produces very different structural, thermodynamic and dynamic effects with implications to ion transport. In IEO/LiTf electrolytes there is an interplay between PEO crystallization and crystalline complex formation with their relative contribution depending strongly on LiTf content. IR revealed a variable degree of ion association in IEO/LiTf polymer electrolytes with higher fraction of free Li-ions at low salt doping and with more complexed species at higher salt concentrations, involving different types of anion/cation aggregates. On the other hand, incorporation of EMITf does not induce complexation indicating a much weaker interaction of PEO with EMI^+ and Tf^- ions the latter being uncoordinated or "free".

Invariably, salt doping increases block copolymer domain spacing in a quantitatively similar way for a given IEO molecular weight. This effect has different origins; in the case of LiTf the increase in domain spacing reflects the increasing effective interaction parameter due to cation complexation and anion solvation effects whereas in the IL case due to swelling. Hence, these systems provide the possibility of studying ion transport under identical domain spacing conditions but in the presence of different interactions/local structures. Because of the different interactions, ion conduction in the two systems was fundamentally different. The measured conductivities in IEO/EMITf were some orders of magnitude higher as compared to the IEO/LiTf case under conditions of identical doping. Furthermore, they displayed an opposite dependence on electrolyte content increasing with EMITf content. In addition to the absolute value of conductivity, the normalized conductivity to the corresponding homopolymer electrolyte showed additional reduction in the LiTf case. Herein, we explored the effect of preferential wetting on the electrodes. We find that preferential wetting of one of the constituent "phases" on the electrodes can lead to a blocking orientation and to a reduced conductivity.

Overall, results presented here suggest that doping of block copolymers with ionic liquids is advantageous over LiTf salts with respect to ion conductivity. The weak interactions of ILs with the polymer backbone as well as their plasticizing role on the segmental dynamics are of key importance in the design of future energy materials. Furthermore, mixing ILs with LiTf electrolytes at appropriate compositions can lead to applications in lithium batteries with superior ion conductivity as compared to the bare LiTf electrolytes.

■ ASSOCIATED CONTENT

Supporting Information

Domain spacing (SAXS), contribution of different ions (IR), temperature dependence of ionic conductivity (DS), and contact angle measurements for different electrodes. This material is available free of charge via the Internet at http://pubs.acs.org.

■ AUTHOR INFORMATION

Corresponding Authors

*(G.F.) E-mail: gfloudas@cc.uoi.gr.
*(E.I.K.) E-mail: eikam@eie.gr.

Notes

The authors declare no competing financial interest.

■ ACKNOWLEDGMENTS

This work was cofinanced by the E.U. European Social Fund and the Greek Ministry of Development-GSRT in the framework of the THALIS program, and the "Excellence in the Research Institutes" program (Projects 64769 and 2005ΣΕ01330081). The current work was also supported by the Research unit on Dynamics and Thermodynamics of the UoI cofinanced by the European Union and the Greek state under NSRF 2007-2013 (Region of Epirus, call 18).

■ REFERENCES

(1) Tarascon, J. M.; Armand, M. *Nature* **2001**, *414*, 359−367 DOI: 10.1038/35104644.
(2) Lodge, T. P. *Science* **2008**, *321*, 50−51.
(3) Armand, M.; Tarascon, J.-M. *Nature* **2008**, *451*, 652−657.
(4) Agrawal, R. C.; Pandey, G. P. *J. Phys. D.: Appl. Phys.* **2008**, *41*, 223001.
(5) (a) Hamley, I. A. In *The Physics of Block Copolymers*; Oxford University Press: Oxford, U.K., 1998. (b) Hadjichristidis, N.; Pispas, S.; Floudas, G. In *Block Copolymers: Synthetic Strategies, Physical Properties and Applications*; Wiley-Interscience: New York, 2002.
(6) Robitaille, C. D.; Fauteux, D. *J. Electrochem. Soc.* **1986**, *133*, 315−325.
(7) Lightfoot, P.; Mehta, M. A.; Bruce, P. G. *Science* **1993**, *262*, 883−885.
(8) Zardalidis, G.; Ioannou, E.; Pispas, S.; Floudas, G. *Macromolecules* **2013**, *46*, 2705−2714.
(9) Kim, S. H.; Misner, M. J.; Yang, L.; Gang, O.; Ocko, B. M.; Russell, T. P. *Macromolecules* **2006**, *39*, 8473−8479.
(10) Singh, M.; Odusanya, O.; Wilmes, G. M.; Eitouni, H. B.; Gomez, E. D.; Patel, A. J.; Chen, V. L.; Park, M. J.; Fragouli, P.; Iatrou, H.; Hadjichristidis, N.; Cookson, D.; Balsara, N. P. *Macromolecules* **2007**, *40*, 4578−4585.
(11) Gomez, E. D.; Panday, A.; Feng, E. H.; Chen, V.; Stone, G. M.; Minor, A. M.; Kisielowski, C.; Downing, K. H.; Borodin, O.; Smith, G. D.; Balsara, N. P. *Nano Lett.* **2009**, *9*, 1212−1216.
(12) Panday, A.; Mullin, S.; Gomez, E. D.; Wanakule, N.; Chen, V. L.; Hexemer, A.; Pople, J.; Balsara, N. P. *Macromolecules* **2009**, *42*, 4632−4637.
(13) Young, W.-S.; Brigandi, P. J.; Epps, T. H., III *Macromolecules* **2008**, *41*, 6276−6279.
(14) Young, W.-S.; Epps, T. H., III *Macromolecules* **2009**, *42*, 2672−2678.
(15) Young, W.-S.; Kuan, W.-F.; Epps, T. H., III *J. Polym. Sci., Part B: Polym. Phys.* **2014**, *52*, 1−16.

DOI: 10.1021/acs.macromol.5b00089
Macromolecules 2015, 48, 1473−1482

(16) Young, W.-S.; Epps, T. H., III *Macromolecules* **2012**, *45*, 4689−4697.
(17) Yuan, R.; Teran, A. A.; Gurevitch, I.; Mullin, S. A.; Wanakule, N. S.; Balsara, N. P. *Macromolecules* **2013**, *46*, 914−921.
(18) Teran, A. A.; Balsara, N. P. *J. Phys. Chem. B* **2014**, *118*, 4−17.
(19) Teran, A. A.; Mullin, S. A.; Hallinan, D. T., Jr.; Balsara, N. P. *ACS Macro Lett.* **2012**, *1*, 305−309.
(20) Nakamura, I.; Balsara, N. P.; Wang, Z.-G. *Phys. Rev. Lett.* **2011**, *107*, 198301−1−5.
(21) Nakamura, I.; Wang, Z.-G. *Soft Matter* **2012**, *8*, 9356−9367.
(22) Nakamura, I.; Wang, Z.-G. *ACS Macro Lett.* **2014**, *3*, 708−711.
(23) Armand, M.; Endres, F.; MacFarlane, D. R.; Ohno, H.; Scrosati, B. *Nat. Mater.* **2009**, *8*, 621−629.
(24) Galinski, M.; Lewandowski, A.; Stepniak, I. *Electrochim. Acta* **2006**, *51*, 5567−5580.
(25) Kumar, Y.; Hashmi, S. A.; Pandey, G. P. *Solid State Ionics* **2011**, *201*, 73−80.
(26) Singh, B.; Sekhon, S. S. *Chem. Phys. Lett.* **2005**, *414*, 34−39.
(27) Costa, L. T.; Lavall, R. L.; Borges, R. S.; Rieumont, J.; Silva, G. G.; Ribeiro, M. C.C. *Electrochim. Acta* **2007**, *53*, 1568−1574.
(28) Singh, P. K.; Kim, K.-W.; Rhee, H.-W. *Synth. Met.* **2009**, *159*, 1538−1541.
(29) Choi, I.; Ahn, H.; Park, M. J. *Macromolecules* **2011**, *44*, 7327.
(30) Hoarfrost, M.; Segalman, R. A. *Macromolecules* **2011**, *44*, 5281.
(31) Gwee, L.; Choi, J. H.; Winey, K. I.; Elabd, Y. A. *Polymer* **2010**, *51*, 5516−5524.
(32) Simone, P. M.; Lodge, T. P. *Macromolecules* **2008**, *41*, 1753−1759.
(33) Virgili, J. M.; Hexemer, A.; Pople, J. A.; Balsara, N.; Segalman, R. A. *Macromolecules* **2009**, *42*, 4604−4613.
(34) Floudas, G.; Vazaiou, B.; Schipper, F.; Ulrich, R.; Wiesner, U.; Iatrou, H.; Hadjichristidis, N. *Macromolecules* **2001**, *34*, 2947−2957.
(35) Floudas, G.; Ulrich, R.; Wiesner, U. *J. Chem. Phys.* **1999**, *110*, 652−663.
(36) (a) Hadjichristidis, N.; Iatrou, H.; Pispas, S.; Pitsikalis, M. *J. Polym. Sci., Part A: Polym. Chem.* **2000**, *38*, 3211−3234. (b) Uhrig, D.; Mays, J. W. *J. Polym. Sci., Part A: Polym. Chem.* **2005**, *43*, 6179−6222.
(37) (a) Esswein, B.; Möller, M. *Angew. Chem., Int. Ed. Engl.* **1996**, *35*, 623−625. (b) Förster, S.; Kramer, E. *Macromolecules* **1999**, *32*, 2783−2785. (c) Pispas, S. *J. Polym. Sci., Part A: Polym. Chem.* **2006**, *44*, 606−613.
(38) Brandrup, J.; Immergut, E. H.; Grulke, E. A. In *Polymer Handbook*; John Wiley and Sons: New York, 1999.
(39) Bolte, M.; Lerner, H.-W. *Acta Crystallogr.* **2001**, *E57*, m231−m232.
(40) (a) Vercher, E.; Orchilles, A. V.; Miguel, P. J.; Martinez-Andreu, A. *J. Chem. Eng. Data* **2007**, *52*, 1468−1482. (b) Garcia-Miaja, G.; Troncoso, G.; Romani, L. *J. Chem. Thermodyn.* **2009**, *41*, 161−166.
(41) Kremer, F.; Schönhals, A. *Broadband Dielectric Spectroscopy*; Springer: Berlin, 2002.
(42) Floudas, G. Dielectric Spectroscopy. In *Polymer Science: A Comprehensive Reference*; Matyjaszewski, K., Möller, M., Eds.; Elsevier BV: Amsterdam, 2012; Vol. 2.32, pp 825−845.
(43) Dyre, J. C. *J. Appl. Phys.* **1988**, *64*, 2456−2468.
(44) Shin, J.-H.; Henderson, H.; Passerini, S. *Electrochem. Commun.* **2003**, *5*, 1016.
(45) Kumar, Y.; Hashmi, S. A.; Panday, G. P. *Electrochim. Acta* **2011**, *56*, 3864−3873.
(46) Xu, J. J.; Ye, H.; Huang, J. *Electrochem. Commun.* **2005**, *7*, 1309−1317.
(47) Cheng, S. Z. D.; Wunderlich, B. *J. Polym. Sci., Part B: Polym. Phys.* **1986**, *24*, 577−594.
(48) Dissanayake, M. A. K. L.; Frech, R. *Macromolecules* **1995**, *28*, 5312−5319.
(49) Frech, R.; Huang, W. *Macromolecules* **1995**, *28*, 1246−1251.
(50) Manning, J.; Frech, R. *Polymer* **1992**, *33*, 3487−3484.
(51) Schantz, S.; Torell, L. M. *Solid State Ionics* **1993**, *60*, 47−53.
(52) Takahashi, Y.; Tadokoro, H. *Macromolecules* **1973**, *6*, 672−675.
(53) Mondal, J.; Choi, E.; Yethiraj, A. *Macromolecules* **2014**, *47*, 438−446.
(54) Parveen, N.; Schonhoff, M. *Macromolecules* **2013**, *46*, 7880−7888.
(55) Noro, A.; Tomita, Y.; Shinohara, Y.; Sageshima, Y.; Walish, J. J.; Matsushita, Y.; Thomas, E. L. *Macromolecules* **2014**, *47*, 4103−4109.

DOI: 10.1021/acs.macromol.5b00089
Macromolecules 2015, 48, 1473−1482